THE UNIVERSITY OF MICHIGAN

INDUSTRY PROGRAM OF THE COLLEGE OF ENGINEERING

AN INVESTIGATION OF CORNER EDDIES

AND

FREE-SURFACE INSTABILITY

Aris C. Spengos

A dissertation submitted in partial fulfillment
of the requirements for the degree of
Doctor of Philosophy in the
University of Michigan
1959

October, 1959

IP-387

Doctoral Committee:

Professor Victor L. Streeter, Co-Chairman
Professor Chia-Shun Yih, Co-Chairman
Associate Professor Jack A. Borchardt
Professor Ernest F. Brater
Professor Jack R. Britton

ACKNOWLEDGMENTS

The writer wishes to express his gratitude and deep appreciation to Professor C. S. Yih not only for his guidance, numerous suggestions and criticisms during this investigation, but also for the inspiration and scientific enthusiasm which the writer enjoyed during his association with Professor Yih.

Appreciation and gratitude is also extended to Professors V. L. Streeter and E. F. Brater for their willingness to review the manuscript before its final typing. The writer also wishes to thank his Doctoral Committee as a whole for their cooperation in supervising his work.

This investigation was partly supported by funds of the Technical Association of Pulp and Paper Industry made available through the UMRI Project No. 2719. The writer wishes to thank the representatives of this organization for their cooperation.

TABLE OF CONTENTS

LIST OF ILLUSTRATIONS

I. INTRODUCTION

The formation of eddies at the corners immediately preceding an abrupt contraction in the flow area, the instability of a free surface due to a downward acceleration, and the instability of a free surface due to an abrupt change in boundary geometry, are the phenomena investigated in the present study.

These phenomena have often been observed in the flow of paper stock in a Fourdrinier paper machine and, among other things, affect adversely the quality of the paper produced. Corner eddies form in the head box of the machine just ahead of the discharge opening. At this location there is an abrupt reduction in the flow area. The presence of these eddies, along with other disturbances in the head box, gives rise to the continuous shedding of vortices which upon their emergence from the discharge opening with a relatively high longitudinal velocity, take the form of vortex tubes. Because the depth of flow after the discharge opening is small (of the order of one inch), these vortex tubes frequently manifest themselves as surface disturbances. Such disturbances not only disturb the even distribution of the pulp fibers but also provide the initial perturbations that are amplified as a result of the subsequent free-surface instability.

The free-surface instability of the paper stock occurs in the vicinity of the table rolls of the Fourdrinier paper machine. These rolls support the wire-screen of the machine on which the paper stock is carried, the whole arrangement resembling an open channel with a

movable bottom. The elasticity of the wire-screen, along with the downward suction that it experiences at a table roll, causes a small amount of wrapping of the wire-screen on the periphery of the table roll downstream from its center. This wrapping of the wire-screen, and its subsequent abrupt rise, provide, respectively, the necessary downward acceleration and abrupt change in boundary geometry which cause the amplification of the surface disturbances emanating from the head box. The amount of wrapping and the speed of the paper stock and wire-screen determine the rate of the amplification of the disturbances. Higher speeds and slacker wire-screen produce greater amplification.

In the investigation of the free-surface instability the region downstream from the top of a table roll has been divided into two parts. The region at which the wire-screen partially wraps on the table roll is referred to as the region with a downward acceleration, the acceleration being the centripetal acceleration of the fluid as it flows around a convex surface. The remaining region is referred to as the region with an abrupt change in boundary geometry.

A few other instances of the occurrence of these phenomena may be mentioned here. The formation of eddies in the flow of a viscous fluid in a channel or pipe with an abrupt contraction in the flow area at the corners immediately preceding that contraction has been observed frequently. The instability of a free surface when accelerated in the direction of the denser fluid has also been found to be relevant to such phenomena as underwater explosions and rocket combustion. In the case of the underwater explosions, an expanding

sphere of gas provides the free surface and the proper acceleration; the amplification of the disturbances in the interface plays an important part in the possible break-up of such bubbles. In the rocket combustion problem the behavior of the free surface of a combustible liquid may play a controlling part in a rocket's performance; the particular type of rocket which will be affected by this phenomenon consists of a combustion chamber originally filled with a combustible liquid. Rapid increase of the surface area of the fluid, due to the amplification of disturbances as the rocket accelerates, will cause a more rapid burning of the fuel to take place and hence, an even further increase in the acceleration.

In Chapter II the effect of rotationality of the upstream flow on the formation of a corner eddy in the head box of a Fourdrinier paper machine is analytically demonstrated. Two-dimensional flow with two different conditions at the discharge opening of the head box were considered; in the first the discharge opening is replaced by a line sink, and in the second by a finite slot. For both conditions the velocity of the flow was assumed to have a sine distribution far upstream from the discharge opening. This assumption was necessary in order to obtain a linear differential equation. Since one is looking for the effect of the non-uniformity of the upstream velocity distribution, the assumption of a sine distribution can advantageously illustrate the effect of upstream rotationality of flow on eddy formation although such a distribution is different from that for uniform flow (turbulent or laminar) in a channel.

In Chapter III the analytical and experimental investigation of the two types of the free-surface instability encountered on the wire-screen of a Fourdrinier paper machine is presented. For the instability due to downward acceleration, an analysis considering the effects of surface tension and depth of fluid, but neglecting those of the Coriolis accelerating and of viscosity, has been carried out for three-dimensional disturbances. This analysis also includes the effects of higher order terms in the differential equations; thus, a non-linear solution of the problem is obtained. In the case of the instability of a free surface due to an abrupt change in the boundary geometry, the lack of a theory made it necessary to resort to a dimensional analysis of the problem. This analysis provided a guide for experimentation.

The experimental equipment built for the investigation of the two types of free-surface instability closely resembles a section of a Fourdrinier paper machine; a head box and a single table roll, without a moving wire-screen, were built. The wrapping of the wire-screen was simulated by a step on the bottom of the channel immediately after the table roll, and water was used in place of paper stock.

II. CORNER EDDIES

The formation of eddies at the corners immediately preceding an abrupt contraction in a conduit, in which a viscous fluid is flowing is a consequence of the rotationality of the flow far upstream and the subsequent action of viscosity. To demonstrate the effect of upstream rotationality on eddy formation, Yih[7] obtained the exact solutions of the governing differential equation for the cases, (a) of a two-dimensional flow with a line sink symmetrically located with respect to the longitudinal boundary, and (b) of an axis-symmetric flow with a point sink located on the axis of symmetry. In these solutions viscosity was considered only as far as its effect in producing rotationality of the flow is concerned, and it was neglected in setting up the differential system.

In the following parts of this chapter the differential systems (with appropriate boundary conditions for the flow in the head box) and their exact solutions for two cases of two-dimensional flow, different from those mentioned above, will be presented.

A. Head Box with Asymmetric Line Sink

The head box under consideration can be described as a two-dimensional conduit of width equal to unity and terminating in a wall with a line sink located asymmetrically at the corner. Such a head box resembles that of a Fourdrinier paper machine with the line sink replacing the discharge opening. The trace of the line sink is

taken as the origin of a Cartesian system of coordinates, with the y-axis extending along the wall, and the negative x-axis extending along the lower boundary of the conduit (see Figure 3).

Making the same assumptions as those mentioned previously, i.e., rotational flow of an inviscid fluid, and if ψ is Lagrange's stream function, the equation[4, p. 244] governing the two-dimensional flow is:

$$\nabla^2\psi = \frac{\partial^2\psi}{\partial x^2} + \frac{\partial^2\psi}{\partial y^2} = f(\psi) \,. \qquad (1)$$

Equation (1) states that the z-component of the vorticity along a streamline is constant and is therefore a function of ψ only.

The velocity distribution far upstream from the sink should be parabolic if a laminar flow of a viscous fluid is considered. But a parabolic distribution of the upstream velocity would make Equation (1) non-linear and thus preclude the possibility of a simple solution. Instead, it is assumed that the velocity distribution far upstream has a sine distribution, which is a distribution nearly parabolic but makes Equation (1) linear. Such an assumption can be tolerated since one is seeking to find the effect of non-uniformity of the upstream velocity on the flow pattern in the vicinity of the line sink. If U_{max} is the velocity at the center line of the head box, i.e. at half-width, the dimensionless upstream velocity is then

$$u = \frac{U}{U_{max}} = \sin \pi y \,, \qquad (2)$$

which vanishes at $y = 0$, and $y = 1$. The corresponding dimensionless

stream function upstream is then

$$\psi = \int_0^{y} -\sin \pi y \, dy = \frac{1}{\pi} \cos \pi y - \frac{1}{\pi} \tag{3}$$

Substituting Equation (3) in Equation (1), one has, for a section far upstream,

$$\nabla^2 \psi = -\pi \cos \pi y . \tag{4}$$

But $\cos \pi y = \pi \psi$ from Equation (3), (if $-\frac{1}{\pi}$ is neglected), thus

$$f(\psi) = -\pi^2 \psi , \tag{5}$$

which is valid not only far upstream but also everywhere downstream, since the vorticity remains constant along a stream line. Equation (1) then becomes

$$\nabla^2 \psi = -\pi^2 \psi \tag{6}$$

and is valid for the whole field of flow, far upstream as well as near the line sink.

If ψ is dimensionless, and L is the length of the head box, the boundary conditions for ψ are:

(i) $\psi \to \frac{1}{\pi} \cos \pi y$ as $x \to -L$,

(ii) $\psi = -\frac{1}{\pi}$ for $x \leq 0$ and $y = 1$,

(iii) $\psi = \frac{1}{\pi}$ for $x < 0$ and $y = 0$,

(iv) $\psi = -\frac{1}{\pi}$ for $x = 0$ and $y > 0$.

Now, to take care of the conditions near the line sink one may assume that

$$\psi = \frac{1}{\pi} \cos \pi y + \psi_1 \,. \tag{7}$$

Substitution of Equation (7) in Equation (1) yields

$$\nabla^2 \psi_1 = -\pi^2 \psi_1 \quad , \tag{8}$$

and the boundary conditions for ψ_1 are

(i) $\psi_1 \to 0$ for $x \to -L$,

(ii) $\psi_1 = 0$ for $x \leq 0$ and $y = 1$,

(iii) $\psi_1 = 0$ for $x < 0$ and $y = 0$,

(iv) $\psi_1 = -\frac{1}{\pi} - \frac{1}{\pi} \cos \pi y$ for $x = 0$ and $0 < y \leq 1$.

The boundary conditions for ψ_1 were obtained by consideration of Equation (7) and the boundary conditions for ψ .

Solution of Equation (8) by the method of separation of variables[2] yields

$$\psi_1 = C_1 \left(1 + \frac{x}{L}\right) \sin \pi y + \sum_{n=2}^{\infty} C_n \left[e^{\pi (n^2-1)^{1/2} x} - e^{-\pi (n^2-1)^{1/2} (2L+x)}\right] \sin n\pi y \tag{9}$$

and is valid for $0 \geq x \geq -L$. This limitation on the values of x was found necessary in order to obtain a Fourier series type of solution. Equation (9) satisfies Equation (8) and the boundary conditions (i), (ii), and (iii) for ψ_1 . The coefficients C_1 and C_n are determined from the boundary condition (iv) for ψ_1 in the following manner:

$$C_1 = 2\int_0^1 -\frac{1}{\pi}(1+\cos\pi y)\sin\pi y\,dy = -\frac{4}{\pi^2},$$

and

$$C_n = 2\int_0^1 -\frac{1}{\pi}(1+\cos\pi y)(1-e^{-2\pi L(n^2-1)^{1/2}})\sin n\pi y\,dy$$

$$= \frac{(-2)}{n\pi^2(n^2-1)}(2n^2+\cos n\pi-1)(1-e^{-2\pi L(n^2-1)^{1/2}})$$

for $n = 2, 3, 4, \ldots$.

Thus, the stream function ψ defining the flow pattern in a head box, or conduit, of length L is

$$\psi = \frac{1}{\pi}\cos\pi y - \frac{4}{\pi^2}\left(1+\frac{x}{L}\right)\sin\pi y + \tag{10}$$

$$+\sum_{n=2}^{\infty} C_n\left[e^{\pi(n^2-1)^{1/2}x} - e^{-\pi(n^2-1)^{1/2}(2L+x)}\right]\sin n\pi y$$

The flow pattern for $L = 5$ is shown in Figure 3(a), in which the corner eddy is evident. The point of separation is of course at $x = -5$, because at this section the velocity has been assumed to have a sine distribution.

B. Head Box with Finite Slot

The geometry of the head box considered in this part is the same as that in the previous case except that the line sink at the origin has been replaced by a two-dimensional finite slot opening of width B. Thus, the head box has now a closer resemblance to that of a Fourdrinier paper machine.

The velocity far upstream is again assumed to have a sine distribution, while the horizontal component of the velocity at the slot is assumed to have a cosine distribution. If $U_{h_{max}}$ is the velocity at the bottom of the slot, the dimensionless horizontal component of the velocity at the slot is then

$$u_h = \frac{U_h}{U_{h_{max}}} = C \cos \frac{\pi y}{2B} \tag{11}$$

and vanishes at $y = B$, while it has the value C at $y = 0$. To determine C the continuity equation is used in the following manner:

$$\psi'_{y=0} - \psi'_{y=1} = C \int_0^B \cos \frac{\pi y}{2B} \, dy = \frac{2BC}{\pi},$$

in which the stream function values are taken at $x = -L$. From the previous part, for a sine distribution of the velocity far upstream, the value of ψ is

$$\psi' = \frac{1}{\pi} \cos \pi y,$$

therefore

$$\frac{2}{\pi} = \frac{2BC}{\pi}, \quad \text{or} \quad C = \frac{1}{B},$$

and

$$u_h = \frac{1}{B} \cos \frac{\pi y}{2B}. \tag{12}$$

The boundary conditions for ψ' are

(i) $\psi' \to \frac{1}{\pi} \cos \pi y$ as $x \to -L$

(ii) $\psi' = -\frac{1}{\pi}$ for $x \leq 0$ and $y = 1$,

(iii) $\psi' = \frac{1}{\pi}$ for $x<0$ and $y=0$,

(iv) $\psi' = -\frac{1}{\pi}$ for $x=0$ and $B \leq y \leq 1$.

Again, in order to take care of the conditions near the slot opening one may assume that

$$\psi' = \frac{1}{\pi} \cos \pi y + \psi_1', \tag{13}$$

and consequently

$$\nabla^2 \psi_1' = -\pi^2 \psi_1' . \tag{14}$$

The boundary conditions for ψ_1' in this case are

(i) $\psi_1' \to 0$ as $x \to -L$,

(ii) $\psi_1' = 0$ for $x \leq 0$ and $y = 1$,

(iii) $\psi_1' = 0$ for $x<0$ and $y=0$,

(iv) $\psi_1' = -\frac{1}{\pi} - \frac{1}{\pi} \cos \pi y$ for $x=0$ and $B \leq y \leq 1$,

and for $x = 0$ and $0 \leq y \leq B$, ψ_1' is obtained from the assumed distribution of the horizontal component of the velocity at the slot and the boundary condition of ψ' at this section; therefore, this yields

$$\psi_1' = \int_0^y -C \cos \frac{\pi y}{2B} \, dy + \frac{1}{\pi} - \frac{1}{\pi} \cos \pi y .$$

So, the last boundary condition is

(v) $\psi_1' = -\frac{2}{\pi} \sin \frac{\pi y}{2B} + \frac{1}{\pi} - \frac{1}{\pi} \cos \pi y$

for $x = 0$ and $0 \leq y \leq B$.

Solution of Equation (14) by the method of separation of variables[2] yields

$$\psi_1' = C_1'\left(1+\frac{X}{L}\right)\sin\pi y + \\ + \sum_{n=2}^{\infty} C_n'\left[e^{\pi(n^2-1)^{1/2}X} - e^{-\pi(n^2-1)^{1/2}(2L+X)}\right]\sin n\pi y, \tag{15}$$

which is the same as Equation (9) and satisfies Equation (14) and the above boundary conditions for ψ_1'.

The coefficients C_1' and C_n' are determined from the boundary conditions (iv) and (v) for ψ_1':

$$C_1' = 2\int_B^1 -\frac{1}{\pi}(1+\cos\pi y)\sin\pi y\,dy + \\ + 2\int_0^B -\frac{1}{\pi}\left(2\sin\frac{\pi y}{2B} - 1 + \cos\pi y\right)\sin\pi y\,dy,$$

$$C_1' = -\frac{4\cos\pi B}{\pi^2(1-4B^2)},$$

and

$$C_n' = 2\int_B^1 -\frac{1}{\pi}(1+\cos\pi y)\left(1-e^{-2\pi L(n^2-1)^{1/2}}\right)\sin n\pi y\,dy + \\ + 2\int_0^B -\frac{1}{\pi}\left(2\sin\frac{\pi y}{2B} - 1 + \cos\pi y\right)\left(1-e^{-2\pi L(n^2-1)^{1/2}}\right)\sin n\pi y\,dy,$$

$$C_n' = \left[-\frac{2+2\cos n\pi}{n\pi^2(n^2-1)} - \frac{4\cos n\pi B}{n\pi^2(1-4B^2n^2)} \right] \left(1 - e^{-2\pi L(n^2-1)^{1/2}}\right),$$

for $n = 2, 3, 4, \ldots\ldots$.

Thus, the stream function ψ' defining the flow pattern in a head box with a slot opening of width B is

$$\psi' = \frac{1}{\pi}\cos\pi y - \frac{4\cos\pi B}{\pi^2(1-4B^2)}\left(1+\frac{x}{L}\right)\sin\pi y + \sum_{n=2}^{\infty} C_n' \left[e^{\pi(n^2-1)^{1/2}x} - e^{-\pi(n^2-1)^{1/2}(2L+x)} \right] \sin n\pi y. \tag{16}$$

The flow pattern for $L = 5$ and $B = 0.15$ is shown in Figure 3(b), in which the corner eddy is again evident.

C. Discussion of Results

A comparison of the two flow patterns in Figure 3, indicates that for $B = 0.15$ there is very small difference in the size of the corner eddies. Therefore, the use of a line sink is justified for discharge openings of small width. For large discharge openings it is expected that the corner eddy will be smaller.

The analyses in this section clearly indicate that the formation of the corner eddies is partly a consequence of the rotationality of the flow.

In the design of the apparatus used for the experimental study of the instability phenomenon it was found necessary to modify the

head box in such a way that the space that would have been occupied by the corner eddy was blocked-off by modification of the upper boundary.

The asymmetric location of the line sink, or slot opening, made it necessary to specify a finite value of x at which the velocity has the assumed distribution, if a simple Fourier series type of solution is desirable. This limitation was not necessary in the cases considered by Yih[7]. Similar limitations are necessary in the solution of many problems of mathematical physics.

The solution of the basic differential equation, Equation (1),

$$\frac{\partial^2 \psi}{\partial x^2} + \frac{\partial^2 \psi}{\partial y^2} = f(\psi)$$

for actual velocity distributions, i.e. when this equation is non-linear, can be accomplished with the use of computing machines, or the method of relaxation. It should be kept in mind though, that no matter how realistic a solution of Equation (1) might be, still it does not govern the flow inside the eddies. This is so because the flow of the eddies does not originate far upstream. The details of the flow inside the eddies may be different from those given by solutions of Equation (1). Thus, solutions of Equation (1) are likely to be valid only for the region outside the corner eddies at high Reynolds numbers (since viscous effects have been only partially taken into account).

III. FREE-SURFACE INSTABILITY

The instability considered in this chapter is that observed on the free surface of the paper stock as it flows over the table rolls of a Fourdrinier paper machine. Small disturbances on the free surface are greatly amplified as the flow of the stock carries them over the table rolls. The area over which this amplification occurs can be divided into two regions, the region directly above the table roll and that downstream from it. In the former, the partial wrapping of the wire-screen around the table roll, caused by the slackness of the wire-screen and the suction at the table roll, subjects the free surface of the paper stock to the full centripetal acceleration due to the rotation of the table roll; since the arc over which this acceleration is applied is relatively small, and it is located immediately downstream from the top of the table roll, one could refer to this region as that with a downward acceleration. Downstream from the table roll, the wire-screen travels in an almost horizontal direction. Over this second region farther amplification of the disturbances occur without the apparent application of an external acceleration. Thus, the amplification appears to be caused by the abrupt change of the boundary geometry.

In the following parts of this chapter, the above described regions of amplification are considered separately. The analyses, as well as the experiments, refer to the experimental apparatus (see Figure 1),

which simulates the operation of one table roll of a Fourdrinier paper machine, with water as the fluid.

A. Free-Surface Instability with Downward Acceleration

The instability of a free surface of a fluid when it is subjected to a downward acceleration larger than that of gravity was first investigated by Taylor[5]. Since then approximately a dozen papers have appeared dealing with this subject. A review of most of these papers is given by Watson[6].

In dealing with the instability problem, Taylor predicted that the interface between two fluids will be always unstable when accelerated in the direction from the lighter toward the heavier fluid with an acceleration larger than that of gravity. To determine stability, Taylor used a method of small perturbations; he considered that the otherwise flat surface has a small sinusoidal displacement at time zero. With the application of an acceleration in the proper direction, these small waves were found to increase in amplitude, with the shortest waves growing faster.

Taylor's work, as well as that of the others, dealt with two-dimensional perturbation, and with fluids of infinite depth. In the following analysis three-dimensional perturbations will be considered, and the effect of the depth of the fluid, and that of the surface tension, will be included.

The downward acceleration that the fluid of thickness d (see Figure 2-a) experiences as it passes over the table roll of the experimental apparatus is

$$a = \omega^2 r_o \,, \tag{17}$$

in which r_o is the radius of the table roll, and ω is its angular speed. The angular speed of the table roll is adjusted so that

$$U = \omega r_o \,, \tag{18}$$

in which U is the mean velocity of the flow in the channel. In dealing with the behavior of fluids which have a mean acceleration and are also acted upon by gravity, it is convenient to replace the acceleration by an equivalent gravity; the mean position of the free surface will be considered stationary in an accelerating coordinate system, and the fluid will be considered as being acted upon by a virtual gravity field which is the sum of the earth's gravitational field and the gravity equivalent of the applied acceleration[3]. In the case under consideration, neglecting the effect of curvature of the cylinder, the problem can be treated as one in which a layer of fluid with thickness d is turned upside down, Figure 2(b), with the solid boundary on top, and is acted upon by a virtual gravitational acceleration of

$$g' = a - g \,, \tag{19}$$

in which g is the actual gravitational acceleration exerted by the earth.

If the viscosity of the fluid is neglected, and the motion is assumed irrorational, the Laplace equation

$$\phi_{xx} + \phi_{yy} + \phi_{zz} = 0, \tag{20}$$

in which subscripts indicate partial differentiation, must be satisfied by the velocity potential ϕ for the disturbances. The boundary condition at the solid boundary is, with u, v, and w denoting the velocity components in the direction of increasing x, y, and z,

$$w = -\phi_z = 0, \text{ at } z = d. \tag{21}$$

The kinematic condition at the free surface is, for a frame moving with velocity U ,

$$\frac{D\eta}{Dt} = \eta_t - \phi_x \eta_x - \phi_y \eta_y = -\phi_z, \text{ at } z = \eta, \tag{22}$$

in which η is the deviation (in the z - direction) from the mean surface, and t is the time. The pressure just inside the free surface is

$$P = P_a + T\left(\frac{1}{R_1} + \frac{1}{R_2}\right), \tag{23}$$

in which p_a is the atmospheric pressure, T is the surface tension, and R_1 and R_2 are the principal radii of curvature. For finite surface disturbances, one has[1, p.169]

$$\frac{1}{R_1} + \frac{1}{R_2} = \frac{\partial}{\partial x}\left(\frac{\eta_x}{M}\right) + \frac{\partial}{\partial y}\left(\frac{\eta_y}{M}\right), \tag{24}$$

where $M=(1+\eta_x^2+\eta_y^2)^{1/2}$. Substitution of Equation (24) in Equation 23) yields

$$P = P_a + T\left[\frac{\partial}{\partial x}\left(\frac{\eta_x}{M}\right) + \frac{\partial}{\partial y}\left(\frac{\eta_y}{M}\right)\right] . \tag{25}$$

On the other hand, Bernoulli's equation yields, with ρ denoting the density,

$$\frac{P}{\rho} = \phi_t - g'\eta - \frac{1}{2}\left(\phi_x^2 + \phi_y^2 + \phi_z^2\right) + C , \tag{26}$$

so that the dynamic boundary condition to be satisfied at the free surface is, combining Equations (25) and (26),

$$\frac{T}{\rho}\left[\frac{\partial}{\partial x}\left(\frac{\eta_x}{M}\right) + \frac{\partial}{\partial y}\left(\frac{\eta_y}{M}\right)\right] = \phi_t - g'\eta - \frac{1}{2}\left(\phi_x^2 + \phi_y^2 + \phi_z^2\right) , \tag{27}$$

if the constant C is taken to be $\frac{P_a}{\rho}$.

Solution of the differential system consisting of Equations (20), (21), (22), and (27) will yield the equations for ϕ and η , which will describe the motion of the free surface.

In the following paragraphs the linear and non-linear solutions of the above system will be presented.

1. Linear Solution

If the higher order terms are omitted, Equation (22) takes the form

$$\eta_t = -\phi_z \quad , \quad \text{at } z = \eta \quad . \tag{22a}$$

To linearize the dynamic boundary condition, the squared terms in the expression

$$M = (1 + \eta_x^2 + \eta_y^2)^{1/2}$$

are dropped and thus M becomes equal to unity. Likewise, the velocity squared terms in Bernoulli's equation are dropped, and Equation (27) becomes

$$\frac{I}{\rho}(\eta_{xx} + \eta_{yy}) = \phi_t - g'\eta \,, \quad \text{at } z = \eta \,. \tag{27a}$$

The linearized differential system, then, consists of Equations (20), (21), (22a), and (27a), and describes the motion of three-dimensional disturbances. The expression for ϕ_1 that satisfies such a system (with the motion starting from rest) can be obtained by the method of separation of variables[2], and is

$$\phi_1 = c \sinh qt \cosh k(z-d) \cos mx \cos ny \,, \tag{28}$$

in which c is a constant, and

$$k^2 = m^2 + n^2 \,, \tag{29}$$

with $m = 2\pi/\lambda_1$, and $n = 2\pi/\lambda_2$, λ_1 and λ_2 being the wave lengths in the directions of x and y respectively.

The growth rate q, can be readily found from Equations (22a), (27a) and (28) to be

$$q^2 = \left(kg' - \frac{I}{\rho}k^3\right) \tanh kd \,. \tag{30}$$

In the process of simplification in obtaining Equation (30), it was assumed that $\eta \ll d$, and thus $\tanh k(\eta - d) = -\tanh kd$.

The initial three-dimensional disturbance on the free surface can be assumed to be of the form

$$\eta_i = \eta(x, y, 0) = \eta_0 \cos mx \cos ny, \tag{31}$$

which after the application of the downward acceleration takes the form

$$\eta_1 = \eta_1'(t) \cos mx \cos ny. \tag{32}$$

Substitution of Equations (28), and (32) into Equation (27a), and after simplification, yields

$$\eta_1'(t) = \frac{ck}{q} \cosh qt \sinh kd. \tag{33}$$

Again, in the process of simplification it was assumed that $\eta_1 \ll d$, and thus $\cosh k(\eta_1 - d) = \cosh kd$. Substituting Equation (33) into Equation (32) one obtains

$$\eta_1 = \eta_0 \cosh qt \cos mx \cos ny, \tag{34}$$

in which

$$\eta_0 = \frac{ck}{q} \sinh kd,$$

with η_0 denoting the amplitude of the initial disturbance. Dividing Equation (34) by Equation (31) one obtains

$$\frac{\eta_1}{\eta_i} = \cosh qt \quad , \tag{35}$$

which could be referred to as the magnitude of amplification of the initial disturbance.

An inspection of Equation (30) indicates that for certain values of k the growth number q vanishes. These values of k can be readily obtained by equating Equation (30) to zero. Obviously, one such value is $k_c = 0$, while the other is $k_c = \sqrt{g'\rho/T}$. The first value, $k_c = 0$, indicates that for an undisturbed free surface, naturally, the growth problem does not arise. The second value, $k_c = \sqrt{g'\rho/T}$, indicates that for disturbances with values of k larger than k_c this analysis fails to predict their growth.

The value of k for the most unstable disturbance can be obtained by differentiating Equation (30) with respect to k and equating the result to zero:

$$2q\frac{dq}{dk} = 0 = \left(g' - \frac{3T}{\rho}k^2\right)\tanh kd + d\left(g'k - \frac{T}{\rho}k^3\right)\operatorname{sech}^2 kd \, .$$

If it is assumed that kd is very large, one obtains, after simplification,

$$k = \sqrt{\frac{g'\rho}{3T}} \quad , \tag{36}$$

which actually gives the maximum of the curve for Equation (30).

2. Non-Linear Solution

For finite amplitudes of the initial disturbances, the higher order terms in the kinematic and dynamic boundary conditions cannot be ignored. The variable M^{-1} in Equation (27) can be approximated by the first two terms of a binomial expansion with $n = -\frac{1}{2}$.

$$M^{-1} = (1+\eta_x^2+\eta_y^2)^{-1/2} \approx 1-\frac{1}{2}(\eta_x^2+\eta_y^2) \tag{37}$$

Other terms in the expansion are omitted because they are of the fourth and higher orders. Completing the differentiation on the left hand side of Equation (27), and substituting in it Equation (37), one obtains, after simplification,

$$\frac{I}{\rho}\left[\eta_{xx}+\eta_{yy}-\frac{3}{2}\eta_x^2\eta_{xx}-\frac{1}{2}\eta_y^2\eta_{xx}-\frac{1}{2}\eta_x^2\eta_{yy}-\right. \tag{38}$$

$$\left.-\frac{3}{2}\eta_y^2\eta_{yy}-2\eta_x\eta_y\eta_{xy}\right]=\phi_t-g'\eta-\frac{1}{2}(\phi_x^2+\phi_y^2+\phi_z^2).$$

In the process of simplification, terms of the fourth and higher orders have been omitted from Equation (38). With the linear solution as first approximation, omission of such higher order terms limits the non-linear solution to a second and third approximation only.

The non-linear solution of the differential system consisting of Equations (20), (21), (22), and (38) will be constructed in the form of

$$\phi = \phi_1+\phi_2+\phi_3\ , \tag{39}$$

and

$$\eta = \eta_1 + \eta_2 + \eta_3 \,. \tag{40}$$

To obtain the second approximation, only first and second order terms will be considered in Equations (22) and (38). Equation (38) reduces to

$$\frac{I}{\rho}(\eta_{xx}+\eta_{yy}) = \phi_t - g'\eta - \frac{1}{2}(\phi_x^2+\phi_y^2+\phi_z^2), \quad \text{at } z=\eta. \tag{41}$$

Now, substituting

$$\phi = \phi_1 + \phi_2 \,,$$

and

$$\eta = \eta_1 + \eta_2 \,,$$

in Equations (22) and (41), and collecting second order terms only, one obtains, after rearrangement of the terms,

$$\eta_{2t} + [\phi_{2z}]_{z=0} = [\phi_{1x}\eta_{1x} + \phi_{1y}\eta_{1y}]_{z=0} - [\phi_{1z}]_{z=\eta} \tag{42}$$

and

$$\frac{I}{\rho}(\eta_{2xx}+\eta_{2yy}) + g'\eta_2 - [\phi_{2t}]_{z=0} = \tag{43}$$

$$= [\phi_{1t}]_{z=\eta} - \frac{1}{2}[\phi_{1x}^2 + \phi_{1y}^2 + \phi_{1z}^2]_{z=0} \,.$$

The right hand sides of Equations (42) and (43) consist of terms that are functions of the first approximation (linear solution) only. Substituting

$$\phi_1 = \frac{c}{2} e^{qt} \cosh k(z-d) \cos mx \cos ny \,, \tag{44}$$

and

$$\eta_1 = \frac{ck}{2q} e^{qt} \sinh kd \cos mx \cos ny \tag{45}$$

(as obtained in the linear solution) into Equations (42) and (43), one obtains, after simplification

$$\eta_{2t} + [\phi_{2z}]_{z=0} = \frac{c^2}{4} e^{2qt} [G' + H' \cos 2mx + \tag{46}$$

$$+ I' \cos 2ny + J' \cos 2mx \cos 2ny]$$

and

$$\frac{T}{\rho}(\eta_{2xx} + \eta_{2yy}) + g'\eta_2 - [\phi_{2t}]_{z=0} = \frac{c^2}{4} e^{2qt} [C' + \tag{47}$$

$$+ D' \cos 2mx + E' \cos 2ny + F' \cos 2mx \cos 2ny].$$

The coefficients of the right hand sides of Equations (46) and (47) are given in the Appendix along with some of the lengthy details that are involved in the non-linear solution.

It should be mentioned here that the form of ϕ_1 and η_1 as given by Equations (44) and (45) is not exactly the same as that given in Equations (28) and (32). The growth factors sinhqt in Equation (28) and coshqt in Equation (33) have been changed to $\frac{e^{qt}}{2}$. This was done to simplify the somewhat lengthy and involved mathematical procedure in obtaining the second and third approximations. As far as the growth of the disturbances is concerned, the exponential time factor divided by 2 yields approximately the same result as the hyperbolic for large values of qt. But, for values of qt close to zero, and particularly at qt = 0, the change to an exponential factor is not consistent with the assumption that the motion starts from rest. This is because the hyperbolic factors at qt = 0 are considerably different than the exponential. Therefore, in forming the non-linear solution Equations (28) and (32) will be used as the first approximation.

Guided by the form of the terms in the right hand sides of Equations (46) and (47), the second approximations for ϕ and η can be constructed as follows:

$$\phi_2 = \frac{c^2}{4} e^{2qt}\left[B_{00} + B_{20}\cosh 2m(z-d)\cos 2mx + \right.$$

$$+ B_{02}\cosh 2n(z-d)\cos 2ny + \qquad (48)$$

$$\left. + B_{22}\cosh 2k(z-d)\cos 2mx\cos 2ny\right],$$

and

$$\eta_2 = \frac{C^2}{4} e^{2qt}\left[A_{oo} + A_{20}\sinh 2md \cos 2mx + \right.$$

$$+ A_{02}\sinh 2nd \cos 2ny + \qquad (49)$$

$$\left. + A_{22}\sinh 2kd \cos 2mx \cos 2ny\right] .$$

The wave numbers of the hyperbolic factors involving the depth of the fluid d were determined by substitution of each term of Equation (48) into the Laplace equation. Thus it was made sure that Equation (48) satisfies the Laplace equation. To determine the coefficients of Equations (48) and (49), these expressions for ϕ_2 and η_2, at $z = 0$, are substituted in the left hand sides of Equations (46) and (47); then, terms of the right hand side of each equation (with the known coefficients) are equated to the corresponding terms on the left hand side. Thus, for each pair, A_{ij} and B_{ij} of the unknown coefficients two equations are obtained; the simultaneous solution of these two equations makes it possible to determine the values of the coefficients A_{ij} and B_{ij} in terms of the known right hand side coefficients of Equations (46) and (47). The values of the coefficients for ϕ_2 and η_2 are given in the Appendix.

For the third approximation, the equations

$$\phi = \phi_1 + \phi_2 + \phi_3 ,$$

and

$$\eta = \eta_1 + \eta_2 + \eta_3$$

are substituted in the boundary conditions given by Equations (22) and (38). Collecting third order terms only, one obtains, after rearrangement of terms,

$$\eta_{3t} + [\phi_{3z}]_{z=0} = [\phi_{1x}\eta_{1x} + \phi_{1y}\eta_{1y}]_{z=\eta} + \tag{50}$$

$$+ [\phi_{1x}\eta_{2x} + \phi_{2x}\eta_{1x} + \phi_{1y}\eta_{2y} + \phi_{2y}\eta_{1y}]_{z=0} + [-\phi_{1z} - \phi_{2z}]_{z=\eta},$$

and

$$\frac{T}{\rho}[\eta_{3xx} + \eta_{3yy}] + g'\eta_3 - [\phi_{3t}]_{z=0} = \frac{T}{\rho}\left[\frac{3}{2}\eta_{1x}^2\eta_{1xx} + \right.$$

$$\left. + \frac{1}{2}\eta_{1y}^2\eta_{1xx} + \frac{1}{2}\eta_{1x}^2\eta_{1yy} + \frac{3}{2}\eta_{1y}^2\eta_{1yy} + 2\eta_{1x}\eta_{1y}\eta_{1xy}\right] + \tag{51}$$

$$+ [\phi_{1t} + \phi_{2t}]_{z=\eta} - \frac{1}{2}[\phi_{1x}^2 + \phi_{1y}^2 + \phi_{1z}^2]_{z=\eta}$$

$$- [\phi_{1x}\phi_{2x} + \phi_{1y}\phi_{2y} + \phi_{1z}\phi_{2z}]_{z=0}.$$

Substituting in the right hand sides of the above equations the expressions for ϕ_1, η_1, ϕ_2, and η_2 given by Equations (43), (45), (48) and (49) respectively, and after considerable number of substitutions and simplifications one finally obtains

$$\eta_{3t} + \left[\phi_{3z}\right]_{z=0} = \frac{c^3}{8} e^{3qt} \left[G'' \cos mx \cos ny + \right.$$

$$+ H'' \cos mx \cos 3ny + I'' \cos 3mx \cos ny + \qquad (52)$$

$$\left. + J'' \cos 3mx \cos 3ny \right] ,$$

and

$$\frac{T}{\rho}\left(\eta_{3xx} + \eta_{3yy}\right) + g'\eta_3 - \left[\phi_{3t}\right]_{z=0} = \frac{c^3}{8} e^{3qt} \left[C'' \cos mx \cos ny + \right.$$

$$+ D'' \cos mx \cos 3ny + E'' \cos 3mx \cos ny + \qquad (53)$$

$$\left. + F'' \cos 3mx \cos 3ny \right] .$$

The coefficients of the right hand sides of Equations (52) and (53) are given in the Appendix.

Guided by the form of the terms in the right hand sides of Equations (52) and (53) the third approximations can be constructed as follows:

$$\phi_3 = \frac{c^3}{8} e^{3qt} \left[B_{11} \cosh k(z-d) \cos mx \cos ny + \right.$$

(54)

$$+ B_{13} \cosh \left(m^2 + 9n^2\right)^{1/2} (z-d) \cos mx \cos 3ny +$$

$$+B_{31}\cosh(9m^2+n^2)^{1/2}(z-d)\cos 3mx\cos ny +$$

$$+B_{33}\cosh 3k(z-d)\cos 3mx\cos 3ny\Big] ,$$

and

$$\eta_3 = \frac{c^3}{8}e^{3qt}\Big[A_{11}\sinh kd\cos mx\cos ny +$$
$$+A_{13}\sinh(m^2+9n^2)^{1/2}d\cos mx\cos 3ny +$$
$$+A_{31}\sinh(9m^2+n^2)^{1/2}d\cos 3mx\cos ny +$$
$$+A_{33}\sinh 3kd\cos 3mx\cos 3ny\Big] . \qquad (55)$$

Equation (54) satisfies the Laplace equation. The wave numbers of the hyperbolic factors involving the depth of the fluid d were determined in the same fashion as those for the second approximation.

To determine the coefficients in Equations(54) and (55) the same procedure was used as that for the second approximation. The values of these coefficients as well as details of the process for their determination are given in the Appendix.

An examination of Equations (49) and (55) shows that the second and third harmonics of the wave numbers of the initial disturbances will contribute in the amplitude growth. It is known that such harmonics will tend to make half of the wave narrow and high while the other half broad and shallow. This is in accordance with the

physical observations made in previous experiments where the disturbances take the form of spikes. Thus, the non-linear solution provides the theoretical justification of such a form. Also, in the third approximation it is interesting to note that there is a term with the same wave numbers as those of the initial disturbance; this indicates that there is a feed-back to the linear solution of the problem.

B. Free-Surface Instability Due to Abrupt Change in Boundary Geometry

In a Fourdrinier paper machine immediately after the table roll, the disturbances which already have been amplified while passing over the table roll continue to grow. The rate of growth over this second region is considerably larger than that in the previous. This phenomenon has been found to depend on the speed of the stock as well as the slackness of the wire-screen. Since there is no apparent downward acceleration that is applied to the paper stock, the instability in this region is attributed to the change of the boundary geometry. The stock approaches the table roll in a horizontal path, passes over the table roll, which is a convex boundary, and then follows again a horizontal path after the wire-screen ceases to wrap on the periphery of the table roll. This abrupt change in the geometry from a convex shape to a horizontal causes the further amplification of the disturbances. At present, this type of instability is not amenable to a mathematical analysis. Instead a dimensional analysis has been performed, to guide the experimentation, and is presented in the following paragraphs.

Referring to Figure 2(a), and with the maximum amplitude η_{max} of the disturbance in the flow subsequent to the table roll as the dependent variable, one has

$$\eta_{max} = f(\eta_i, d, h, r_o, U, \rho, T, \mu, g), \quad (56)$$

in which h is the step height, corresponding to the wrapping of the wire-screen, μ is the dynamic viscosity, T the surface tension, and η_i is the initial amplitude of the disturbance measured at the top of the cylinder. In a linear theory the above functional relationship can be simplified to

$$\frac{\eta_{max}}{\eta_i} = f_1(d, h, r_o, U, \rho, T, \mu, g). \quad (57)$$

Using the Π -theorem of dimensional analysis, the independent variables of Equation (57) can be grouped into the dimensionless numbers of the following functional relationship

$$\frac{\eta_{max.}}{\eta_i} = F_1\left(\frac{h}{d}, \frac{r_o}{d}, \frac{T\rho d}{\mu^2}, R, F\right), \quad (58)$$

in which

$$\begin{aligned} R \text{ (Reynolds number)} &= \frac{Ud\rho}{\mu}, \\ F \text{ (Froude number)} &= \frac{U}{\sqrt{gd}}. \end{aligned} \quad (59)$$

In the experiments performed, T, d, r_o, ρ, and μ have been kept constant, so for these experiments,

$$\frac{\eta_{max}}{\eta_i} = F_2\left(\frac{h}{r_o}, R, F\right). \tag{60}$$

If it is assumed that the effect of viscosity can be neglected, the equation to be used for organization of the experimental data reduces to

$$\frac{\eta_{max}}{\eta_i} = F_3\left(\frac{h}{r_o}, F\right). \tag{61}$$

Equation (61) indicates that the growth of the disturbances depends on the radius of curvature of the table roll in terms of h, and on the Froude number.

C. Experimental Apparatus

The experimental apparatus, a sketch of which is shown in Figure 1, was built to simulate flow conditions in a Fourdrinier paper machine. The head box consisted of a conduit 30 inches long with a flow area of 6 inches square. It was connected to the 6 inch pipe of the water supply system of the laboratory, and the flow was regulated through a valve located upstream from the head box. On the top of the head box two bleeding lines provided the necessary passages for removing the trapped air. The formation of a corner eddy was avoided by installing a perforated inclined plate immediately upstream from the discharge opening. This plate, with a bleeding line attached

to the end plate of the head box, made it possible to obtain a relatively undisturbed free surface downstream from the discharge opening. The top and bottom of the head box were made of brass plates of a quarter inch thickness and its sides were made of plexiglass plates three-quarters of an inch thick.

The channel, after the head box, had a brass plate a quarter inch thick as the bottom and side walls made of plexiglass one inch high and a quarter inch thick. The side walls were so adjusted that the width of the channel, within which the flow occurred, was 6 inches wide to match the width of the head box. Every effort was made to avoid abrupt or gradual changes in the channel walls. This was necessary in order to reduce the generation of waves that will be carried downstream because of the high Froude number that characterized the flow.

The table roll consisted of a plexiglass cylinder 8-3/4 inches long and 8.8 inches in diameter; the thickness of the cylinder wall was one quarter of an inch. The shaft of the cylinder, passing through the end plates, was supported by self-aligning ball bearings. A variable speed electric motor drive, connected to the cylinder shaft through pulleys and a V-belt, made it possible to vary the speed of rotation of the cylinder from about zero revolutions per minute up to 600.

The clearance between the table roll and the upstream bottom plate of the channel was approximately 0.035 inch, and that between the table roll and the downstream plate approximately 0.060 inch.

The amount of water leaking from the downstream clearance when the table roll was rotating, was approximately nine percent of the total discharge.

Two water tanks, one underneath the table roll and another at the end of the channel, provided the means by which the discharge through the apparatus was measured.

The initial disturbances on the free surface of the flow were created by saw-teeth (23 teeth in 6 inches) extending along the top of the discharge opening. Each of the saw-teeth was 3/8 inch long and 1/4 inch wide, and they were cut on a 1/32 inch thick brass plate. This plate was attached to the end plate of the head box and by sliding it up or down the size of the exposed teeth could be varied.

The velocity of the water in the channel was measured with a pitot tube located immediately upstream from the table roll and in the middle of the channel. The velocity distribution of the flow upstream from the table roll was approximately uniform. The ratio of the mean velocity, as determined by measuring the discharge and the flow area, to the maximum velocity, as determined by the pitot tube, was about 0.9.

The average amplitude of the disturbance was measured by a point gage that was electrically insulated except of a small length of its tip. A voltage potential was connected across the point gage and the flowing water with the negative terminal of the voltage connected to the point gage. Contact of the top of the point gage

with the crest of the disturbances was indicated by the deflection of the electron beam on the screen of an oscilloscope (the oscilloscope was connected across a resistance in series with the point gage). This indicated the elevation of the crest relative to an arbitrary datum. The elevation of the trough of the disturbances was obtained, similarly, by moving the point gage downward until the continuous electrical contact was interrupted intermittently. An arbitrary number of contacts per second at the crest, and interruptions at the trough, were decided upon as the indication of the respective elevations. This number was kept the same for measurements at the top of the table roll, over the table roll, and downstream from it. Such measurements, of course, did not make it possible to obtain the exact amplitude of the disturbances, but it is hoped that the ratio of the amplitudes η/η_i) was quite accurately determined.

The wave lengths of the disturbances were estimated by visual observation and from photographs taken with the aid of a high speed flashlight with a period of 1/15,000 second.

In preparing the apparatus for the collection of the experimental data, first the speed of rotation of the table roll was set at the desired angular speed and then the flow was adjusted so that its velocity, at the uniform part of the flow, was the same as the peripheral speed of the table roll. Measurement of the depth of flow was made at several locations. The amplitude of the disturbances was measured at the top of the table roll, to determine

the initial value of it, and at several locations over the table roll and downstream from it. The discharge at the end of the channel, and that through the clearances at the table roll, was measured with the use of a weighing tank.

Although the experimental apparatus did not have a moving wire-screen to simulate exactly the flow conditions at a Fourdrinier machine, comparison of pictures taken of an actual machine with those taken of this apparatus indicated that a duplication of the phenomenon was obtained. This was made possible by replacing the wrapping of the wire-screen on the periphery of the table roll, with a step at the bottom of the channel right after the table roll. Thus, the flow in the experimental apparatus followed a convex boundary over the table roll as it does in the case of a Fourdrinier paper machine with a slack wire-screen.

D. Discussion of Results

The experimental data for the growth of the disturbances over the table roll (the region characterized by a downward acceleration) are plotted in Figure 4. For comparison, the linear solution of the differential system, in the form of Equation (35), has been plotted also.

The comparison of the linear solution with the experimental results is based on the following understanding of the initial condition and interpretation of the time t. In the analysis it has been assumed that the flow has a mean velocity U, and it is subjected uniformly to an acceleration g^1. Starting from $t = 0$, the free

surface has a corrugation but the perturbation velocity in the z-direction is assumed to be zero. In the experiments the acceleration was applied to the fluid as it reached the top of the table roll. At this location the time average of the initial amplitude η_i was measured. Subsequent time-average measurements of η were made at various values of x. Thus, the corresponding t was taken to be x/U and it is indicated as such in Figure 4.

The scatter of the experimental points is primarily due to the experimental error in determining the value of k as given by Equation (29). The measurement of the wave lengths of the disturbances was not accurate because of the difficulties involved in making such measurement at high Froude numbers. The experimental error was further magnified in the computation of the growth number q as given by Equation (30). In this equation the term for the effect of the surface tension is proportional to the third power of k. The accuracy for the measurement of the ratio η/η_i was considerably better. Most of the data were taken twice in order to check the reproducibility of this ratio. As it is seen in Figure 4, the variation in such measurements was on the average about 5%. Nevertheless, the experimental results verify the trend predicted by the linear solution.

A comparison of the data shown in Figure 4 with the non-linear solution was not attempted because of the large scatter of the experimental points; furthermore, this solution has been constructed for large values of qt only (greater than 2). It has already been explained, in this chapter, that the hyperbolic growth factors of

the linear solution were replaced by $e^{qt}/2$ in order to facilitate the construction of the non-linear solution. Such a change is contrary to the assumption that motion starts from rest. For large values of qt, however, the exponential growth factor gives approximately the same results as the hyperbolic. Experimental data for values of qt larger than 2 were not obtained because of the limitations of the experimental equipment; for larger values of qt eddies generated in the flow upstream from the head box manifested themselves as violent disturbances on the free surface of the water and made the measurement of the ratio η/η_i very inaccurate.

In an effort to evaluate the non-linear solution, data for two-dimensional disturbances given by Watson[6] were plotted in Figure 5. These data were obtained under considerably better experimental conditions and for large values of qt. His experimental setup consisted of a rectangular container, partly filled with a fluid, which was accelerated downward. Elaborate instrumentation was used to measure the wave length and amplitude of the two-dimensional sinusoidal disturbances. In this case, however, the scatter of the experimental points also is considerable.

The linear and non-linear solutions for the two-dimensional case, plotted in Figure 5, were obtained by substitution of $n = 0$ in the equations for the three-dimensional case. In the non-linear solution only the first and second approximations were used; the tedious and long computations for the third approximation were not considered justifiable after the comparison shown in Figure 5. It can, however, be stated that for values of qt larger

than approximately 4.5, the linear and non-linear solutions give values of amplitude larger than those obtained experimentally.

The experimental data for the growth of the disturbances downstream from the table roll are shown in Figure 6, from which it can be seen that they are consistent with Equation (61). The ratio η_{max}/η_i is indeed increasing with both h/r_o and Froude number. In this region too most of the experimental points were taken twice to check their reproducibility.

Plates I and II show pictures of the growth of the disturbances for the two values of h that were used in the experiments, and for only three values of U. From these pictures it is obvious that the growth of the disturbances downstream from the table roll is considerably larger than that over the table roll. This has also been observed in the operation of the Fourdrinier paper machine. At high speeds of flow ($U = 30$ fps) in a paper machine the disturbances grow to the extent that they break up into drops that jump as high as two feet above the surface of the paper stock.

IV. CONCLUSIONS

From the foregoing chapters of this investigation it can be concluded that:

1. The formation of the corner eddies in the head box of a Fourdrinier paper machine, or in any other conduit with an abrupt contraction, is partly a consequence of the rotationality of the flow.
2. The free-surface instability of the fluid, as it flows directly over the table rolls of a Fourdrinier paper machine, is essentially caused by the downward acceleration induced by the curvature of the wire-screen as it wraps around the table rolls.
3. The free-surface instability occurring downstream from the table rolls is a consequence of the abrupt change in boundary geometry caused by the leveling of the wire-screen subsequent to the partial wrapping of it around the table rolls. The degree of wrapping of the wire has been found to have a pronounced effect on the growth of the disturbances.

For a better evaluation of the mathematical analysis for the growth of the disturbances over the table rolls further experimentation is needed. Better controlled experiments, preferably without a horizontal flow velocity, will provide data for the

determination of the accuracy of the non-linear solution. Also, an adequate mathematical analysis for the growth of the disturbances due to an abrupt change of the boundary geometry is very desirable.

BIBLIOGRAPHY

1. Bateman, H., Partial Differential Equations of Mathematical Physics, Cambridge: At the University Press, 1932, p. 169.

2. Churchill, R. V., Fourier Series and Boundary Value Problems, New York: McGraw-Hill Book Co., 1941.

3. Joos, G. and Freeman, I., Theoretical Physics, 2d edition, New York: Hafner Publishing Co., 1950, p. 229.

4. Lamb, H., Hydrodynamics, New York: Dover Publications, 1945, p. 244.

5. Taylor, Sir Geoffrey, "The Instability of Liquid Surfaces when Accelerated in a Direction Perpendicular to their Planes, I.," Proc. Roy. Soc. (London) A 201 (1950), p. 192.

6. Watson, B. C., "An Experimental Study of Accelerated Fluids (The Taylor Problem)," Interim Technical Report No. 16, Combustion Aerodynamics Project, Division of Engineering and Applied Physics, Harvard University, June 1957.

7. Yih, C. S., "Two Solutions for Inviscid Rotational Flow with Corner Eddies," Journal of Fluid Mechanics, 5, Part 1, (January 1959), p. 36.

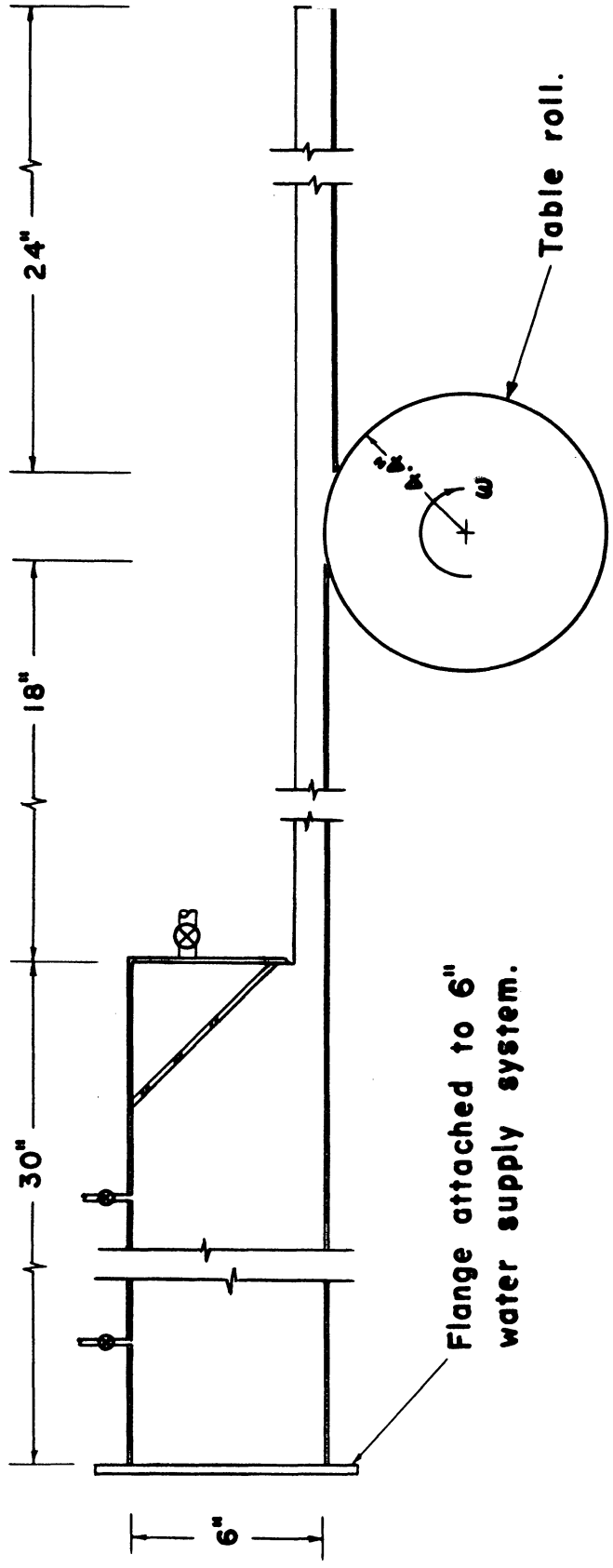

Figure 1. Sketch of the Experimental Apparatus

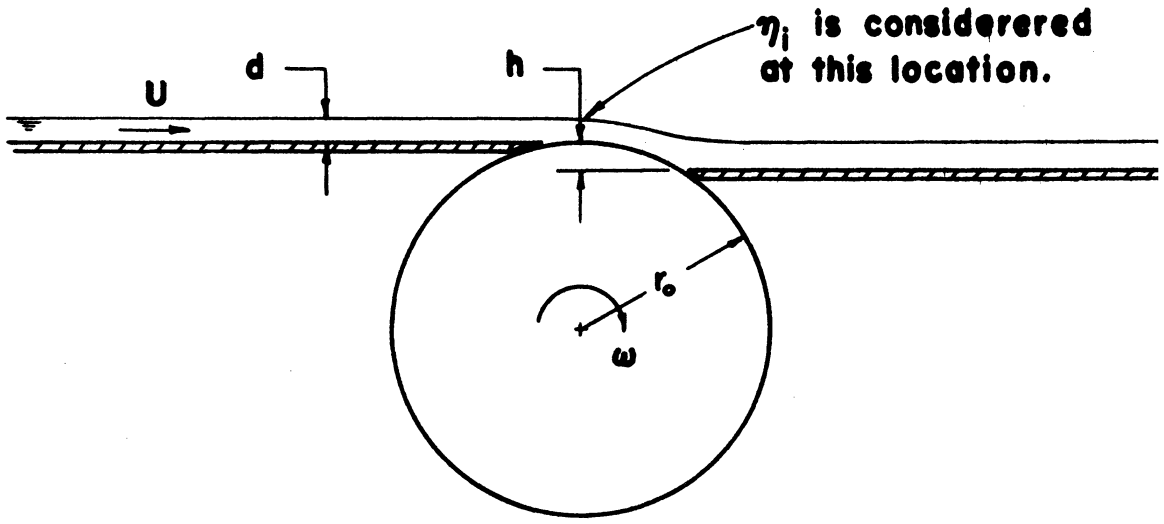

(a)

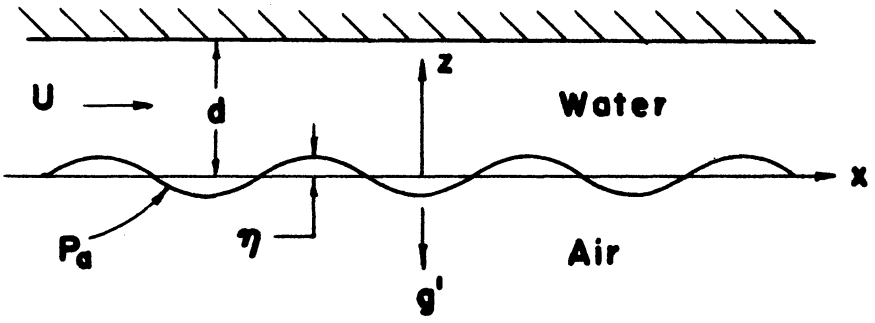

(b)

Figure 2. Definition Sketches

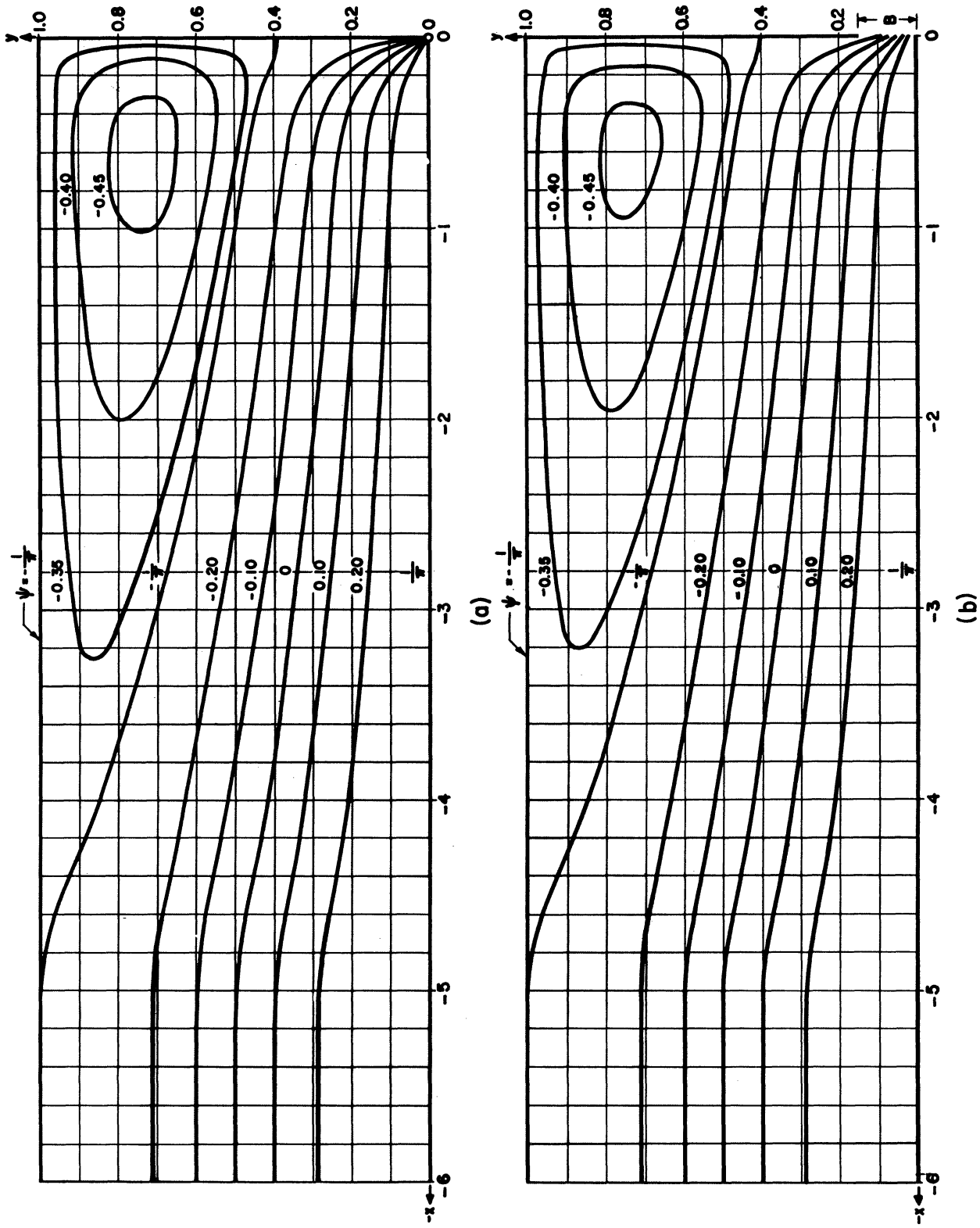

Figure 3. Corner Eddies (a) With a Line Sink, (b) With a Slot

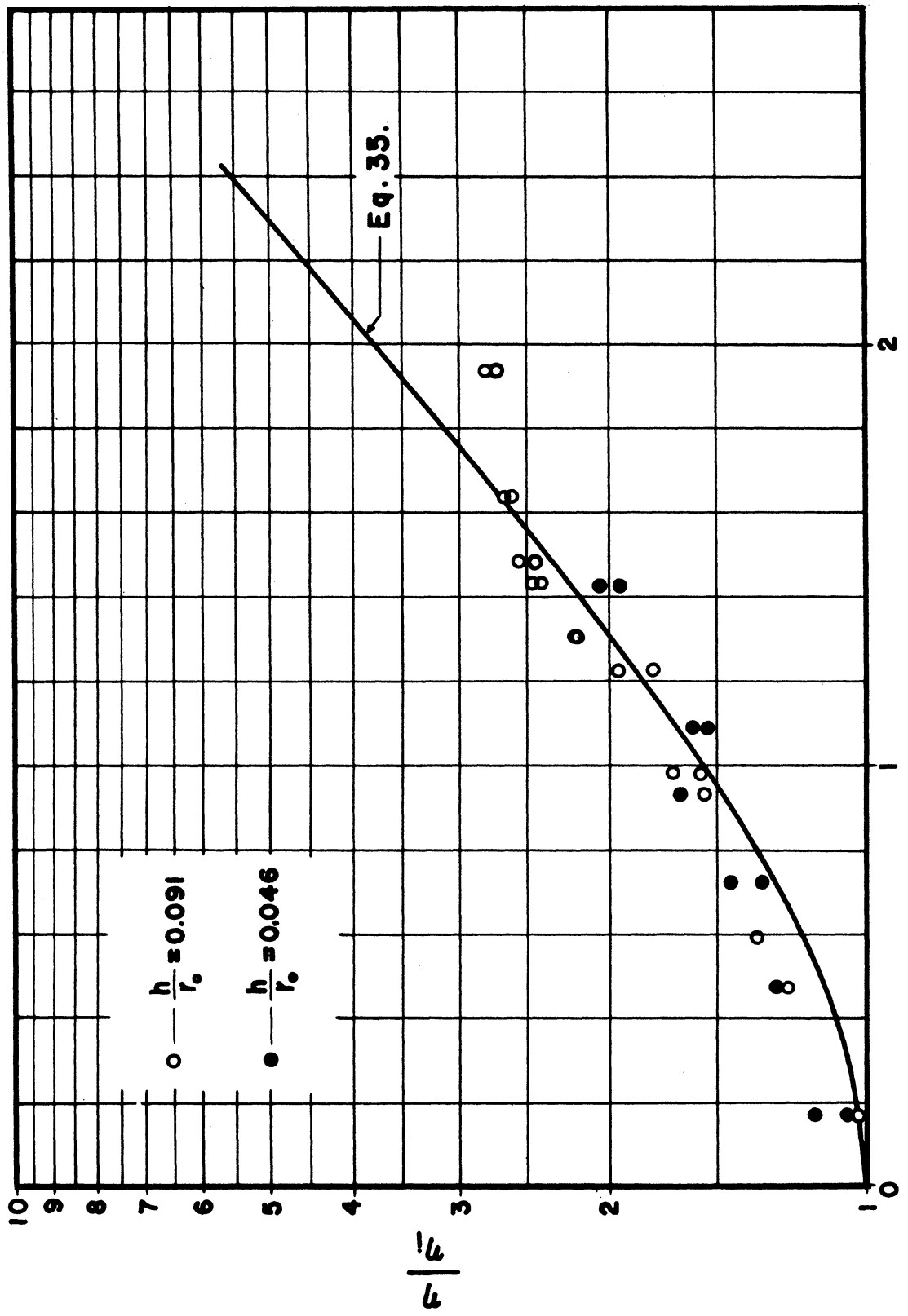

Figure 4. Growth of Disturbances Over the Table Roll

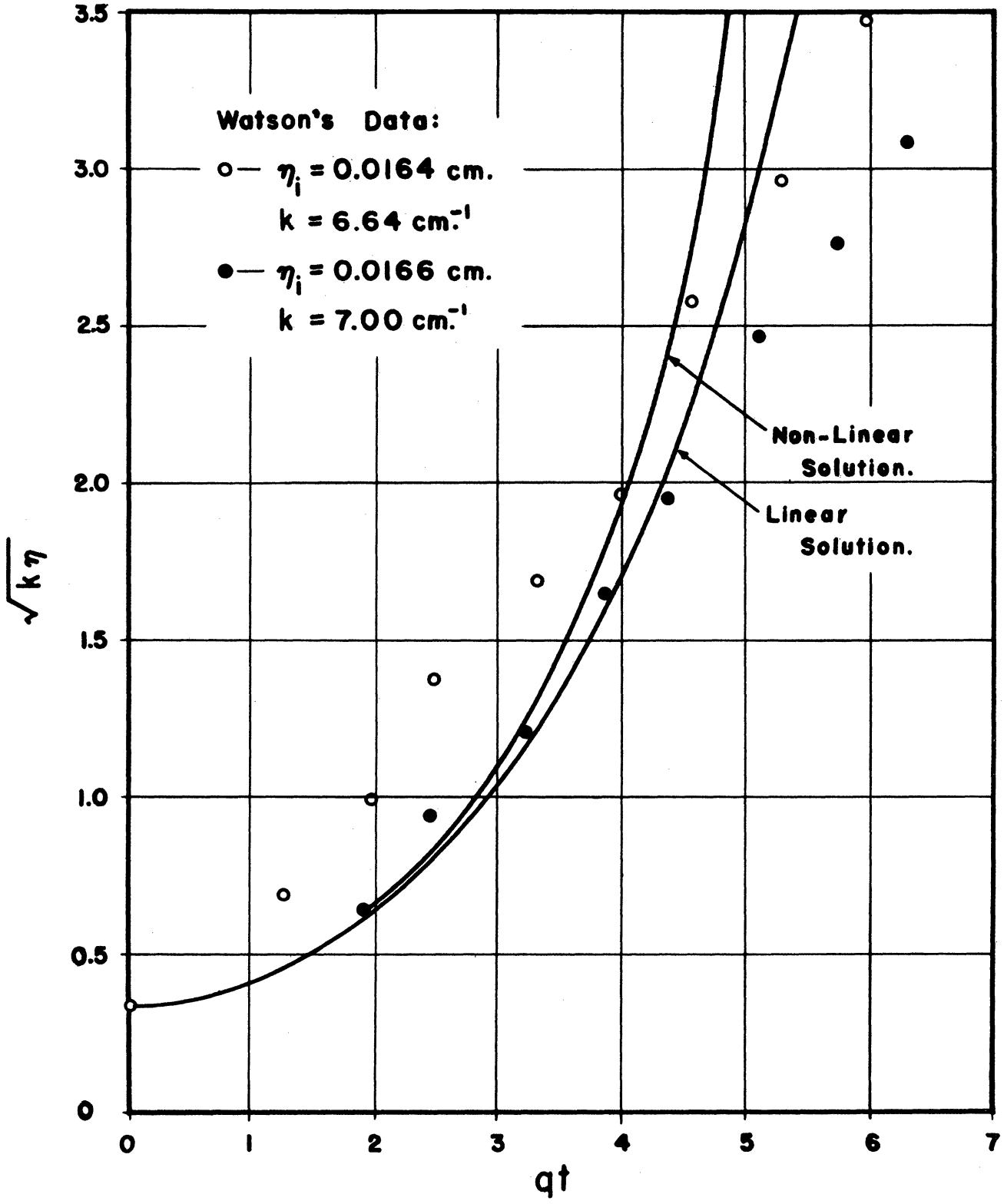

Figure 5. Growth of Two-Dimensional Disturbances

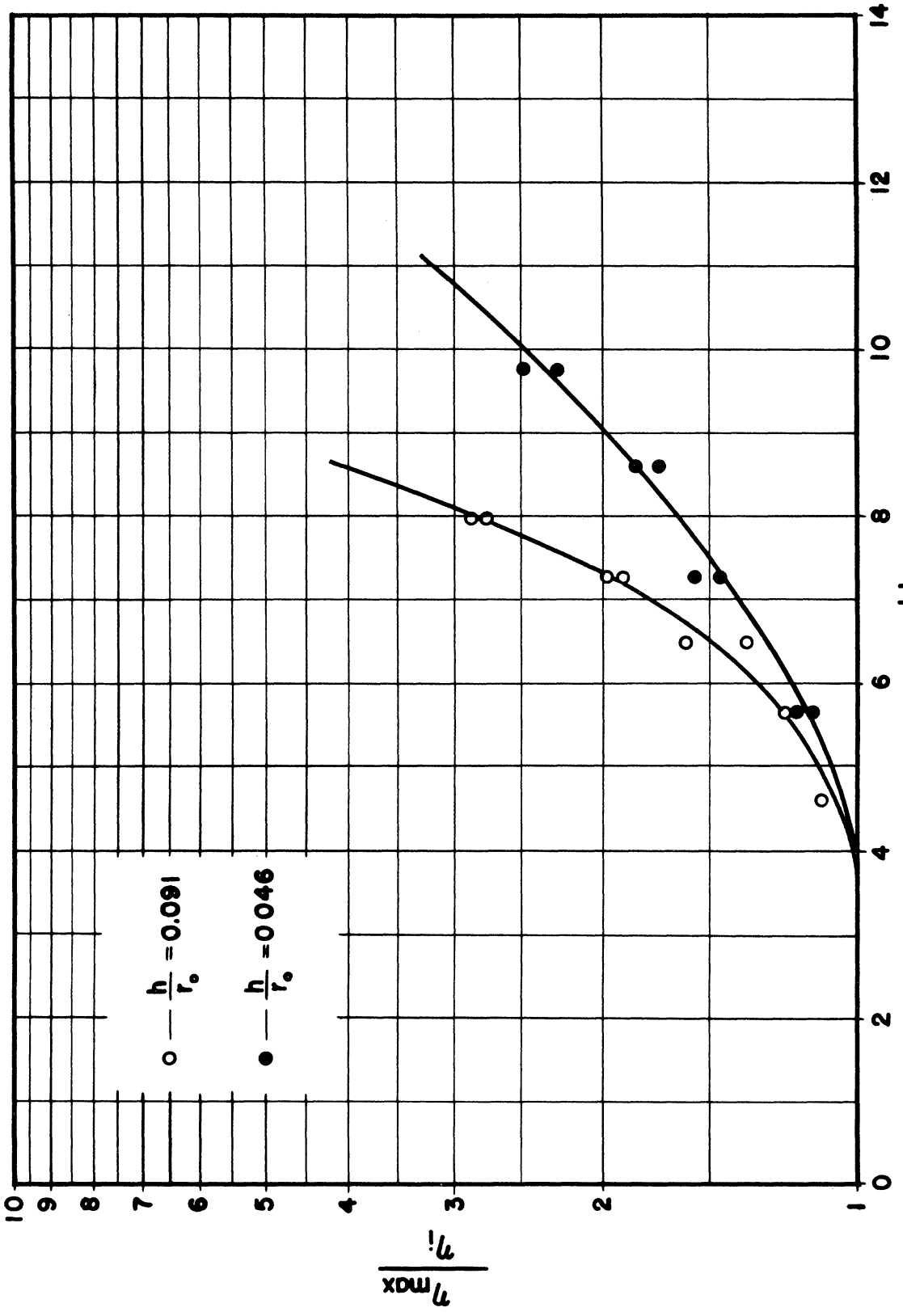

Figure 6. Growth of Disturbances Downstream from the Table Roll

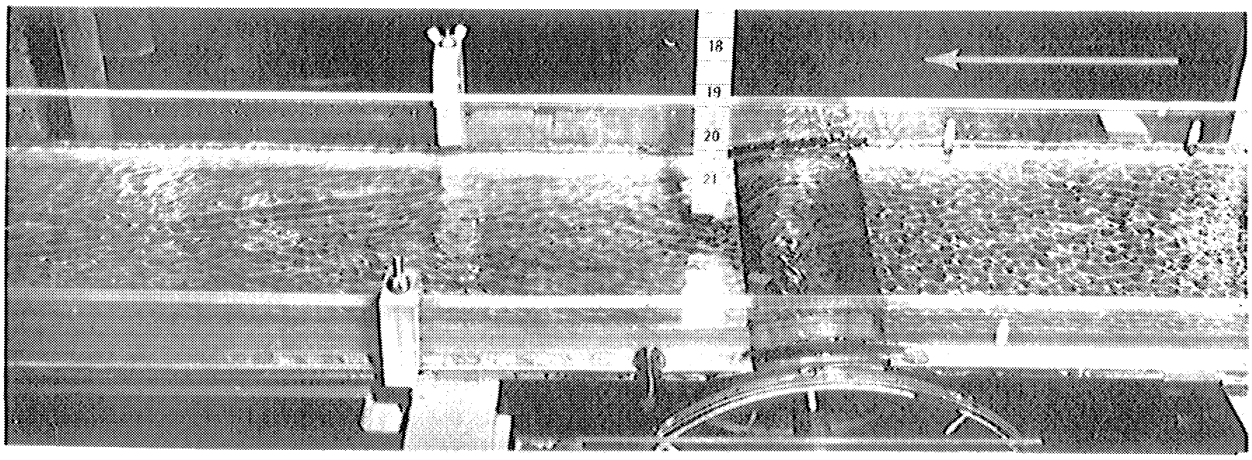

1-d

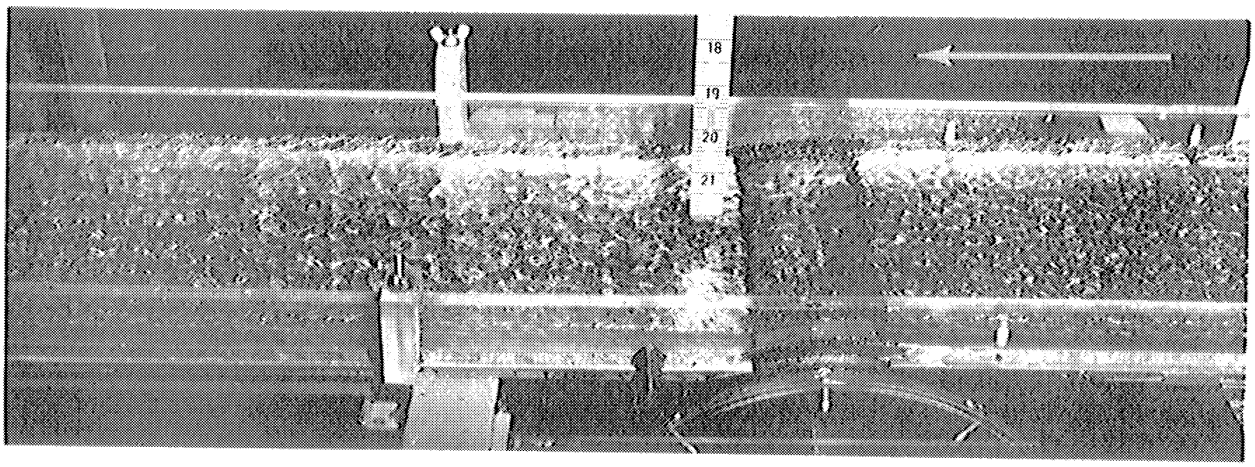

6-d

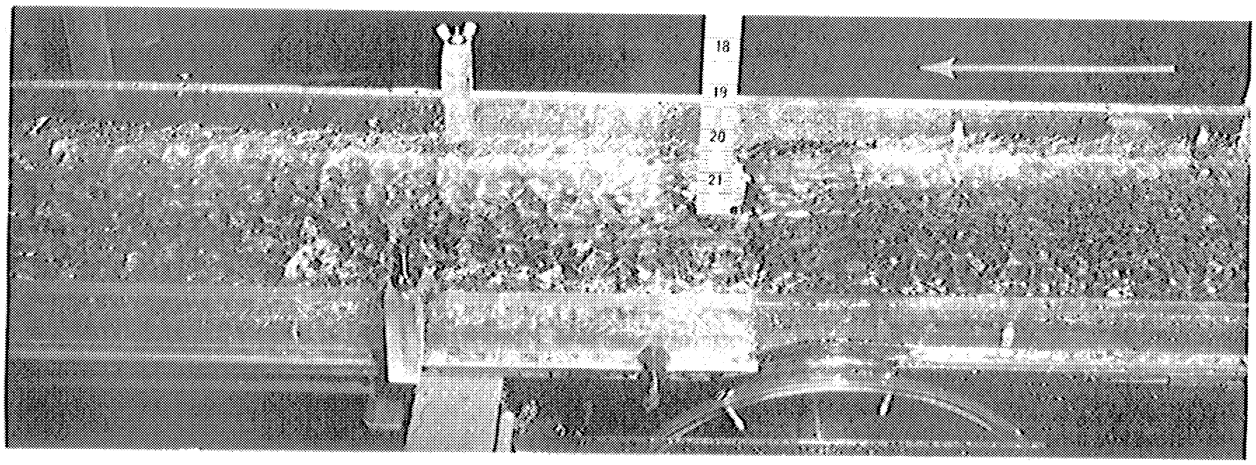

12-d

Plate I. (1-d) g' = 0, h = 0.2 in., U = 3.4 fps, flow is to the left

(6-d) g' = 5.0 g, h = 0.2 in., U = 8.4 fps, flow is to the left

(12-d) g' = 14.0 g, h = 0.2 in., U = 13.3 fps, flow is to the left

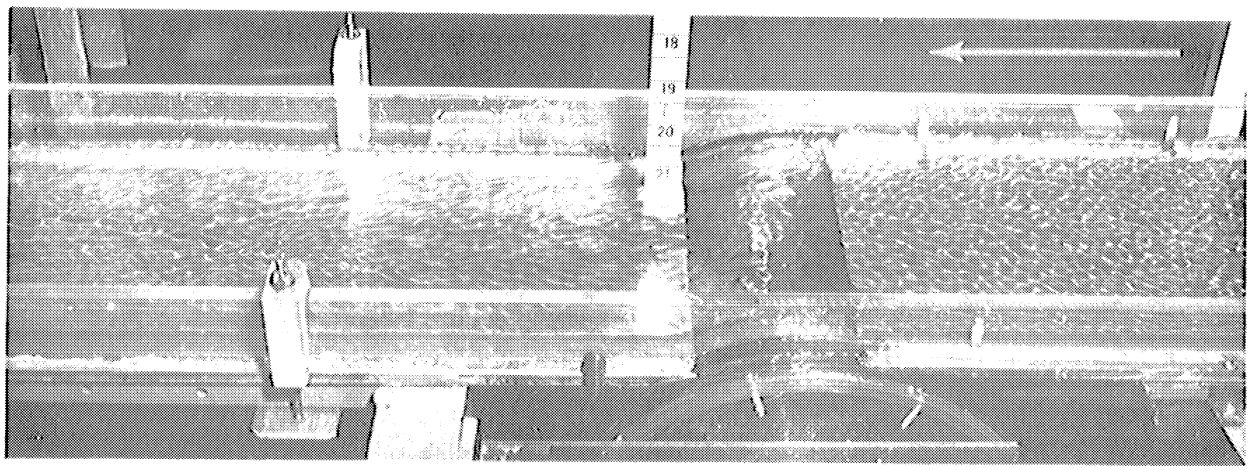

10-c

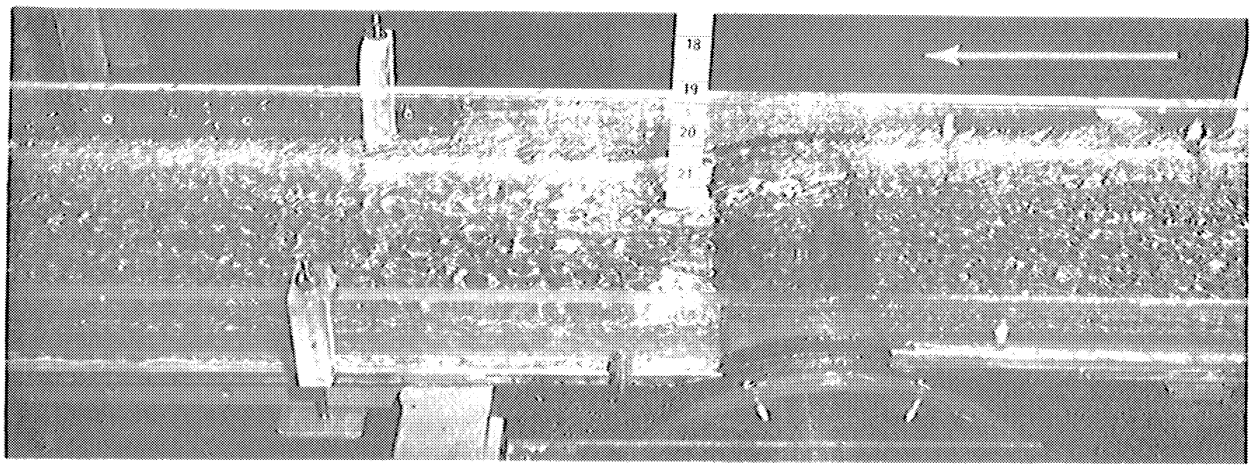

5-c

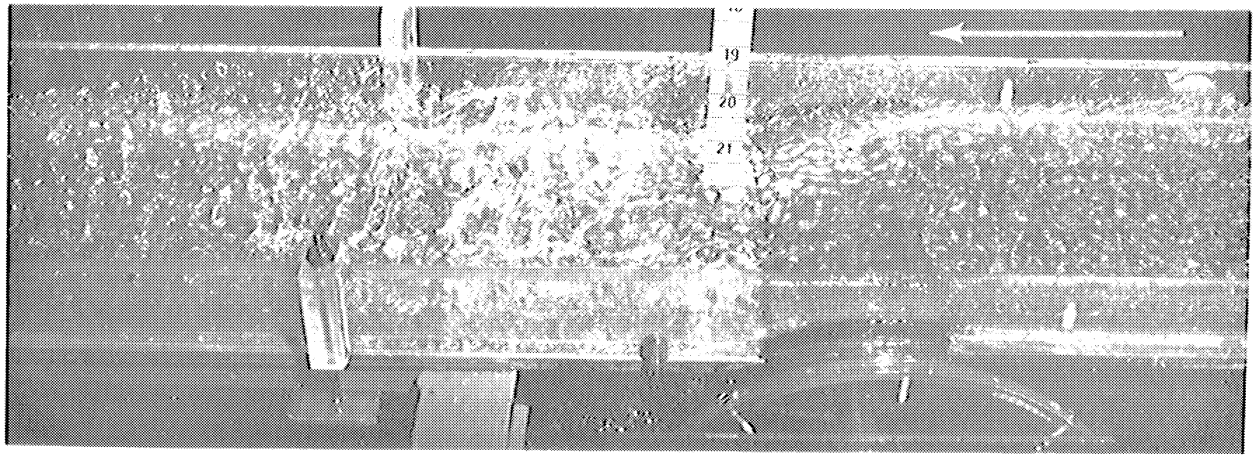

13-c

Plate II. (10-c) g' = 0 h = 0.4 in., U = 3.4 fps, flow is to the left

(5-c) g' = 5.0 g, h = 0.4 in., U = 8.4 fps, flow is to the left

(13-c) g' = 14 0 g, h = 0.4 in., U = 13.3 fps, flow is to the left

APPENDIX

The coefficients, and some of the details, of the non-linear solution of the differential system consisting of Equations (20), (21), (22), and (38) are given below.

Second Approximation

The coefficients of Equations (46) and (47) are:

$$G' = 0$$

$$H' = -\frac{km^2}{4q} \sinh 2kd$$

$$I' = -\frac{kn^2}{4q} \sinh 2kd$$

$$J' = -\frac{k^3}{4q} \sinh 2kd$$

$$C' = -\frac{3k^2}{8} \sinh^2 kd - \frac{1}{8} k^2 \cosh^2 kd$$

$$D' = -\frac{3k^2}{8} \sinh^2 kd + \frac{1}{8} (m^2 - n^2) \cosh^2 kd$$

$$E' = -\frac{3k^2}{8} \sinh^2 kd - \frac{1}{8} (m^2 - n^2) \cosh^2 kd$$

$$F' = -\frac{3k^2}{8} \sinh^2 kd + \frac{1}{8} k^2 \cosh^2 kd$$

The coefficients of Equations (48) and (49) were determined from the following equations:

1) For A_{oo} and B_{oo}

$$A_{oo} g' - B_{oo} 2q = C'$$

$$A_{oo} 2q = G' ,$$

simultaneous solution of these equations yields

$$A_{oo} = 0, \text{ and } B_{oo} = -\frac{C'}{2q} .$$

2) For A_{20} and B_{20}

$$A_{20}\left(q' - \frac{4Tm^2}{\rho}\right)\sinh 2md - B_{20}\,2q\cosh 2md = D'$$

$$A_{20}\,2q\sinh 2md \qquad - B_{20}\,2m\sinh 2md = H',$$

simultaneous solution of these equations yields

$$A_{20} = \frac{H'}{2q\sinh 2md} + \frac{2mD' - H'\frac{m}{q}\left(q' - \frac{4Tm^2}{\rho}\right)}{2m\left(q' - \frac{4Tm^2}{\rho}\right)\sinh 2md - 4q^2\cosh 2md}$$

$$B_{20} = \frac{2qD' - H'\left(q' - \frac{4Tm^2}{\rho}\right)}{2m\left(q' - \frac{4Tm^2}{\rho}\right)\sinh 2md - 4q^2\cosh 2md} .$$

3) For A_{02} and B_{02}

$$A_{02}\left(q' - \frac{4Tn^2}{\rho}\right)\sinh 2nd - B_{02}\,2q\cosh 2nd = E'$$

$$A_{02}\,2q\sinh 2nd \qquad - B_{02}\,2n\sinh 2nd = I'$$

simultaneous solution of these equations yields

$$A_{02} = \frac{I'}{2q\sinh 2nd} \quad \frac{2nE' - I'\frac{n}{q}\left(q' - \frac{4Tn^2}{\rho}\right)}{2n\left(q' - \frac{4Tn^2}{\rho}\right)\sinh 2nd - 4q^2\cosh 2nd}$$

$$B_{02} = \frac{2qE' - I'\left(q' - \frac{4Tn^2}{\rho}\right)}{2n\left(q' - \frac{4Tn^2}{\rho}\right)\sinh 2nd - 4q^2\cosh 2nd} .$$

4) For A_{zz} and B_{zz}

$$A_{zz}\left(q' - \frac{4Tk^2}{\rho}\right)\sinh 2kd - B_{zz}\,2q\cosh 2kd = F'$$

$$A_{zz}\,2q\sinh 2kd \qquad - B_{zz}\,2k\sinh 2kd = J' ,$$

simultaneous solution of these equations yields

$$A_{22} = \frac{J'}{2q\sinh 2kd} + \frac{2kF' - J'\frac{k}{q}\left(q' - \frac{4Tk^2}{\rho}\right)}{2k\left(q' - \frac{4Tk^2}{\rho}\right)\sinh 2kd - 4q^2\cosh 2kd}$$

$$B_{22} = \frac{2qF' - J'\left(q' - \frac{4Tk^2}{\rho}\right)}{2k\left(q' - \frac{4Tk^2}{\rho}\right)\sinh 2kd - 4q^2\cosh 2kd} .$$

Third Approximation

The coefficients of Equation (52) are:

$$G'' = -12a_1 - 2b_1 - 4(c_1 + 3e_1 + f_1 + h_1) + 4(i_1 + \ell_1) + 36p_1 + 4r_1$$

$$H'' = -4(a_1 + c_1) + 12e_1 + 4(f_1 + h_1 + \ell_1) + 12p_1 + 4r_1$$

$$I'' = 12a_1 + 2b_1 + 4(c_1 - e_1 - f_1 + i_1) + 12p_1 + 4r_1$$

$$J'' = 4(a_1 + c_1 + e_1 + f_1 + p_1 + r_1) ,$$

in which

$$a_1 = \frac{k^3m^2}{64q^2}\sinh^3 kd$$

$$b_1 = -\frac{m^2A_{zo}}{4}\cosh kd\sinh 2md - \frac{km^2B_{zo}}{4q}\cosh 2md\sinh kd$$

$$c_1 = -\frac{m^2A_{zz}}{8}\cosh kd\sinh 2kd - \frac{km^2B_{zz}}{8q}\cosh 2kd\sinh kd$$

$$e_1 = \frac{k^3 n^2}{64 q^2} \sinh^3 kd$$

$$f_1 = -\frac{n^2 A_{zz}}{8} \cosh kd \sinh 2kd - \frac{k n^2 B_{zz}}{8q} \cosh 2kd \sinh kd$$

$$h_1 = -\frac{n^2 A_{oz}}{4} \cosh kd \sinh 2nd - \frac{k n^2 B_{oz}}{4q} \cosh 2nd \sinh kd$$

$$i_1 = -\frac{k^2 B_{zo}}{8} \cosh kd \sinh 2md - \frac{k m^2 B_{zo}}{2q} \cosh 2md \sinh kd$$

$$\ell_1 = -\frac{k^2 A_{oz}}{8} \cosh kd \sinh 2nd - \frac{k n^2 B_{oz}}{2q} \cosh 2nd \sinh kd$$

$$p_1 = \frac{k^5}{128 q^2} \sinh^3 kd$$

$$r_1 = -\frac{k^2 A_{zz}}{16} \cosh kd \sinh 2kd - \frac{k^3 B_{zz}}{4q} \cosh 2kd \sinh kd .$$

The coefficients of Equation (53) are:

$$C'' = -12(a_2+b_2) + 4c_2 + 36e_2 + 4(f_2+h_2+i_2) - 2\ell_2 - 4(p_2+r_2+s_2)$$

$$D'' = -4a_2 + 12b_2 - 4c_2 + 12e_2 + 4(i_2 - p_2 + r_2 + s_2)$$

$$E'' = 12a_2 - 4(b_2+c_2) + 12e_2 + 4i_2 + 2\ell_2 + 4(p_2 - s_2)$$

$$F'' = 4(a_2+b_2+c_2+e_2+f_2+h_2+i_2+p_2+s_2),$$

in which

$$a_2 = \frac{T}{\rho 64 q^3}\left(\frac{3k^3m^4}{2} + k^3m^2n^2\right)\sinh^3 kd - \frac{k^2m^2}{64q}\cosh kd \sinh^2 kd$$

$$b_2 = \frac{T}{\rho 128 q^3}(3k^3n^4 + k^3m^2n^2)\sinh^3 kd - \frac{k^2n^2}{64q}\cosh kd \sinh^2 kd$$

$$c_2 = \frac{T}{\rho 32 q^3} k^3m^2n^2 \sinh^3 kd$$

$$e_2 = \frac{3k^4}{128q} \cosh kd \sinh^2 kd$$

$$f_2 = \left(-\frac{kq A_{zo}}{8} - \frac{3km B_{zo}}{4}\right) \sinh kd \sinh 2md$$

$$h_2 = \left(-\frac{kq A_{oz}}{8} - \frac{3kn B_{oz}}{4}\right) \sinh kd \sinh 2nd$$

$$i_2 = \left(-\frac{kq A_{zz}}{16} - \frac{3k^2 B_{zz}}{8}\right) \sinh kd \sinh 2kd$$

$$\ell_2 = \frac{m^2 B_{zo}}{4} \cosh kd \cosh 2md$$

$$p_2 = \frac{m^2 B_{zz}}{8} \cosh kd \cosh 2kd$$

$$r_2 = \frac{n^2 B_{oz}}{4} \cosh kd \cosh 2nd$$

$$s_2 = \frac{n^2 B_{zz}}{8} \cosh kd \cosh 2kd \,.$$

The coefficients of Equations (54) and (55) were determined from the following equations:

1) For A_{11} and B_{11}

$$A_{11}\left(q' - \frac{Tk^2}{\rho}\right) \sinh kd - B_{11}\, 3q \cosh kd = C''$$

$$A_{11}\, 3q \sinh kd \qquad - B_{11}\, k \sinh kd = G'',$$

simultaneous solution of these equations yields

$$A_{11} = \frac{G''}{3q \sinh kd} + \frac{kC'' - G''\frac{k}{3q}\left(q' - \frac{Tk^2}{\rho}\right)}{k\left(q' - \frac{Tk^2}{\rho}\right) \sinh kd - 9q^2 \cosh kd}$$

$$B_{11} = \frac{3qC'' - G''\left(q' - \frac{Tk^2}{\rho}\right)}{k\left(q' - \frac{Tk^2}{\rho}\right) \sinh kd - 9q^2 \cosh kd} \,.$$

2) For A_{13} and B_{13}

$$A_{13}\left[q' - \frac{I}{\rho}(m^2+9n^2)\right]\sinh(m^2+9n^2)^{1/2}d - B_{13}3q\cosh(m^2+9n^2)^{1/2}d = D''$$

$$A_{13}3q\sinh(m^2+9n^2)^{1/2}d \qquad -B_{13}(m^2+9n^2)^{1/2}\sinh(m^2+9n^2)^{1/2}d = H'',$$

simultaneous solution of these equations yields

$$A_{13} = \frac{H''}{3q\sinh(m^2+9n^2)^{1/2}d} + \frac{(m^2+9n^2)^{1/2}D'' - H''\left(\frac{m^2+9n^2}{3q}\right)^{1/2}\left[q' - \frac{I}{\rho}(m^2+9n^2)\right]}{(m^2+9n^2)^{1/2}\left[q' - \frac{I}{\rho}(m^2+9n^2)\right]\sinh(m^2+9n^2)^{1/2}d - 9q^2\cosh(m^2+9n^2)^{1/2}d}$$

$$B_{13} = \frac{3qD'' - H''\left[q' - \frac{I}{\rho}(m^2+9n^2)\right]}{(m^2+9n^2)^{1/2}\left[q' - \frac{I}{\rho}(m^2+9n^2)\right]\sinh(m^2+9n^2)^{1/2}d - 9q^2\cosh(m^2+9n^2)^{1/2}d}.$$

3) For A_{31} and B_{31}

$$A_{31}\left[q' - \frac{I}{\rho}(9m^2-n^2)\right]\sinh(9m^2+n^2)^{1/2}d - B_{31}3q\cosh(9m^2+n^2)^{1/2}d = E''$$

$$A_{31}3q\sinh(9m^2+n^2)^{1/2}d \qquad -B_{31}(9m^2+n^2)^{1/2}\sinh(9m^2+n^2)^{1/2}d = I'',$$

simultaneous solution of these equations yields

$$A_{31} = \frac{I''}{3q\sinh(9m^2+n^2)^{1/2}d} + \frac{(9m^2+n^2)^{1/2}E'' - I''\left(\frac{9m^2+n^2}{3q}\right)\left[q' - \frac{I}{\rho}(9m^2+n^2)\right]}{(9m^2+n^2)^{1/2}\left[q' - \frac{I}{\rho}(9m^2+n^2)\right]\sinh(9m^2+n^2)^{1/2}d - 9q^2\cosh(9m^2+n^2)^{1/2}d}$$

$$B_{31} = \frac{3qE'' - I''\left[q' - \frac{I}{\rho}(9m^2+n^2)\right.}{(9m^2+n^2)^{1/2}\left[q' - \frac{I}{\rho}(9m^2+n^2)\right]\sinh(9m^2+n^2)^{1/2}d - 9q^2\cosh(9m^2+n^2)^{1/2}d}.$$

4) For A_{33} and B_{33}

$$A_{33}\left(q' - \frac{T}{\rho}9k^2\right)\sinh 3kd - B_{33}\,3q\cosh 3kd = F''$$

$$A_{33}\,3q\sinh 3kd \qquad\qquad - B_{33}\,3k\sinh 3kd = J'',$$

simultaneous solution of these equations yields

$$A_{33} = \frac{J''}{3q\sinh 3kd} + \frac{3kF'' - J''\frac{k}{q}\left(q' - \frac{T}{\rho}9k^2\right)}{3k\left(q' - \frac{T}{\rho}9k^2\right)\sinh 3kd - 9q^2\cosh 3kd}$$

$$B_{33} = \frac{3qF'' - J''\left(q' - \frac{T}{\rho}9k^2\right)}{3k\left(q' - \frac{T}{\rho}9k^2\right)\sinh 3kd - 9q^2\cosh 3kd}\,.$$
